ACS APPLIED MATERIALS & INTERFACES

Letter

www.acsami.org

# Solution-Processed Photovoltaics with a 3,6-Bis(diarylamino)fluoren-9-ylidene Malononitrile

Supravat Karak,[†,‡] Paul J. Homnick,[†] Lawrence A. Renna,[†] D. Venkataraman,[†] Joel T. Mague,[§] and Paul M. Lahti*[,†]

[†]Department of Chemistry and [‡]Department of Polymer Science & Engineering, University of Massachusetts, Amherst, Massachusetts 01003, United States

[§]Department of Chemistry, Tulane University, New Orleans, Louisiana 70118, United States

Supporting Information

**ABSTRACT:** 3,6-Bis(*N*,*N*-dianisylamino)-fluoren-9-ylidene malononitrile (FMBDAA36) was used as an electron donor material in solution-processed organic photovoltaic devices with configuration ITO/PEDOT:PSS/(1:3[w/w] FMBDAA36:$PC_{71}BM$)/LiF/Al to give power conversion efficiencies up to 4.1% with open circuit voltage $V_{OC}$ = 0.89 V, short circuit current $J_{SC}$ = 10.35 mA $cm^{-2}$, and fill factor FF = 44.8%. Conductive atomic force microscopy of the active layer showed granular separation of regions exhibiting easy versus difficult hole transport, consistent with bulk heterojunction type phase separation of FMBDAA36 and $PC_{71}BM$, respectively. Single-crystal X-ray diffraction analysis showed pure FMBDAA36 to form columnar $\pi$-stacks with a 3.3 Å intermolecular spacing.

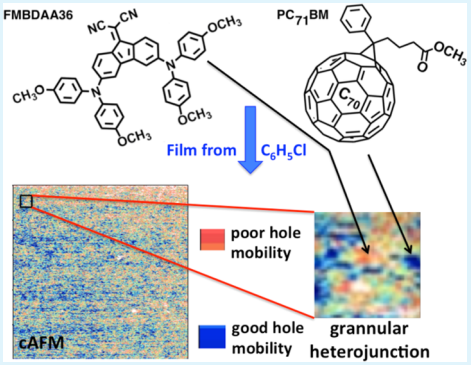


**KEYWORDS:** *organic photovoltaics, small molecule photovoltaics, fluorenylidene malononitrile, conductive atomic force microscopy, solution-processed solar cells*

Small molecules can often be conveniently incorporated into organic photovoltaic (OPV) devices by vapor deposition,[1,2] but recent work increasingly has focused on using solution-fabrication methods[3,4] with potential for industrial up-scaled use. In this letter, we report using 3,6-bis(*N*,*N*-dianisylamino)-fluoren-9-ylidene malononitrile (FMBDAA36) as an effective electron donor material with electron acceptor [6,6]-phenyl-$C_{71}$-butyric acid methyl ester ($PC_{71}BM$) to make all-small-molecule OPV devices with power conversion efficiency (PCE) of about 4% by straightforward spin-coating from a single solvent.

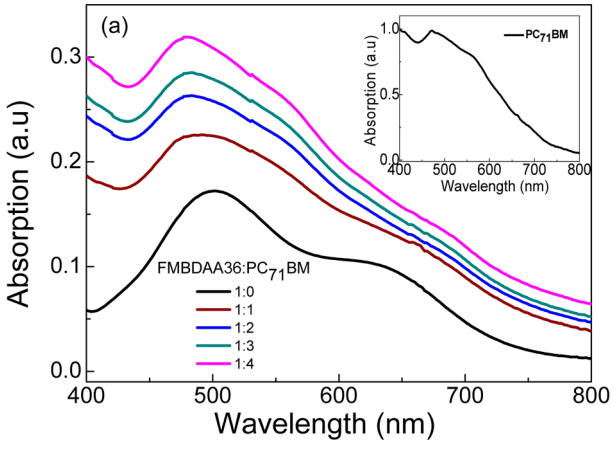


**Figure 1.** Absorbance of solution-processed FMBDAA36:$PC_{71}BM$ films with various blend ratios ranging from 1:0 to 1:4. The film thickness is 110 ± 5 nm. The inset shows absorbance of a neat film of $PC_{71}BM$ for comparison.

FMBDAA36 was designed to be synthetically accessible using the method described by Homnick et al.[5] (see the Supporting Information, Scheme S1 and Figures S1−S2), with a a relatively low energy optical band onset with absorption through most of the visible solar spectrum and with orbital energy levels tuned for effective performance with PCBM electron acceptors. It has broadly overlapping solution absorption spectral band maxima at 483 and 597 nm, with absorption onset at about 720 nm (1.72 eV), as shown in the Supporting Information Figure S3; in the solid state, it appears nearly black. Its longer wavelength molar absorptivity is strengthened to about 4500 $M^{-1}$ $cm^{-1}$ by the dipole-enhancing direct conjugation of its electron rich dianisylamine groups relative to the C═C$(CN)_2$ group of the fluorenylidene malononitrile (FM) unit.[6] Hybrid density functional computations show[5] a major shift in orbital population from the dianisylamine groups in the highest occupied molecular orbital (HOMO) to the FM unit in the lowest unoccupied molecular

Received: July 28, 2014
Accepted: September 23, 2014
Published: September 29, 2014

  

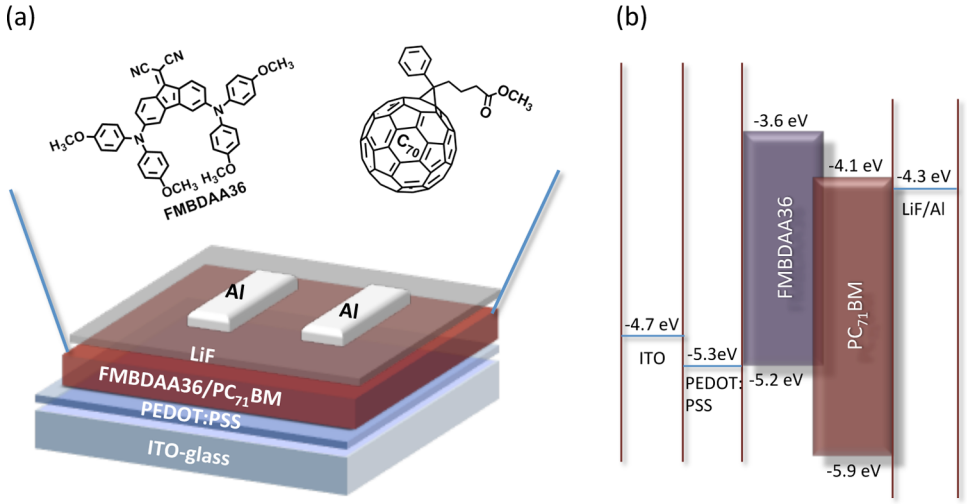


**Figure 2.** (a) Schematic diagram of the device configuration and molecular structure of FMBDAA36 and $PC_{71}BM$. (b) Schematic illustration of energy level diagram of ITO/PEDOT:PSS/FMBDAA36:$PC_{71}BM$/LiF/Al solar cell.

**Table 1. Device Performance Parameters for FMBDAA36:$PC_{71}BM$-Based Solar Cells Using Different Weight Ratios of Material in the Active Layer**

| weight ratio (FMBDAA36:$PC_{71}BM$) | $J_{SC}$ (mA $cm^{-2}$) | $V_{OC}$ (V) | FF (%) | PCE (%) |
|---|---|---|---|---|
| 1:1 | 7.14 (7.02 ± 0.12) | 0.86 (0.84 ± 0.02) | 34.1 (33.2 ± 0.9) | 2.1 (2.0 ± 0.1) |
| 1:2 | 9.09 (9.00 ± 0.09) | 0.87 (0.85 ± 0.02) | 34.2 (33.0 ± 1.2) | 2.7 (2.5[5] ± 0.1[5]) |
| 1:3 | 10.35 (10.21 ± 0.14) | 0.89 (0.88 ± 0.01) | 44.8 (43.4 ± 1.4) | 4.1 (3.9 ± 0.2) |
| 1:4 | 4.18 (4.08 ± 0.10) | 0.90 (0.88 ± 0.02) | 34.3 (33.2 ± 1.1) | 1.3 (1.2 ± 0.1) |

[a]All performance data obtained using devices of configuration ITO/PEDOT:PSS/FMBDAA36:$PC_{71}BM$/LiF/Al, with the FMBDAA36:$PC_{71}BM$ active layers spin coated from chlorobenzene. Best device performance metrics are given; average values with standard deviations shown in parentheses.

orbital (LUMO), indicating substantial charge-transfer nature in the HOMO−LUMO excitation.

The FMBDAA36 used in this study was purified by recrystallization from spectral grade acetonitrile and thorough vacuum drying, or by sublimation at 180 °C under a vacuum of <1 mmHg. These procedures gave small single crystals, of quality sufficient for X-ray diffraction analysis to show an orthorhombic $Pca2_1$ lattice with two very similar but crystallographically distinguishable FMBDAA36 molecules that form parallel, columnar $\pi$-stacks along the *a*-axis. The crystal data and refinement parameters are given in the Supporting Information (Table S1). The dianisylamine groups are both strongly twisted relative to the fluorenylidene unit, which presumably limits delocalization of the amine lone pair onto the fluorenylidene. The fluorenylidene units $\pi$-stack with alternating — but not parallel — $C{=}C(CN)_2$ group alignment, with about 3.3 Å spacing between fluorenylidene units and essentially no stack slippage. Overall, the crystallography of FMBDAA36 has well-separated electron rich (dianisylamine group) and electron depleted (fluorenylidene) regions, in columns when viewed in the *bc*-plane along the *a*-axis (see the Supporting Information, Figure S4). This packing pattern should be conducive to good charge transport due to the chains of $\pi$-cloud contacts among fluorenylidene units and dianisylamine units, separately.

Chlorobenzene is a good solvent for dissolving $PC_{71}BM$ and an adequate solvent for FMBDAA36, allowing codissolution and spin-coating of FMBDAA36:$PC_{71}BM$ mixtures. Thin films of FMBDAA36 absorb broadly over 400−750 nm; codeposition with $PC_{71}BM$ increases absorption for various blend compositions in the 400−450 nm region in accord with the $PC_{71}BM$ spectral profile shown in Figure 1; absorption onset occurs at ∼750 nm (1.65 eV). Ultraviolet photoelectron spectroscopy (UPS) of pure FMBDAA36 thin films gave a HOMO energy of −5.2 eV (see the Supporting Information, Figure S5), from which its LUMO energy was estimated to be −3.6 eV by adding the solid film optical absorption onset energy. Previous solution electrochemical studies in acetonitrile found an oxidation onset potential of 0.279 V and reduction onset potential of −1.060 V (relative to the ferrocene/ferrocenium redox potential): application of the typical empirical relationship $E_{MO}(eV) = -(E_{redox} + 4.8)$ yields electrochemical $E_{HOMO} = -5.1$ eV and $E_{LUMO} = -3.7$ eV. Although electrochemical and UPS $E_{HOMO}$ energies can be different because of the different conditions often used for the different measurements, in this case, the agreement is quite good, showing the value of the molecular engineering strategy used to design[5] the FMBDAA36 energy levels along with its absorption spectrum.

The optimum weight:weight (w:w) ratio of FMBDAA36:$PC_{71}BM$ for maximum power conversion efficiency (PCE) was determined by spin coating various FMBDAA36:$PC_{71}BM$ mixtures (all at 35 mg/mL in chlorobenzene) to form mixed-component active layers in ITO/PEDOT:PSS/ (FMBDAA36:$PC_{71}BM$)/LiF/Al configuration OPV test devices. Further details of device fabrication and characterization are described in the Supporting Information. Figure 2 shows the device configuration and component energy levels obtained from the UPS and optical band gaps for thin films of both FMBDAA36 and $PC_{71}BM$. In particular, UPS

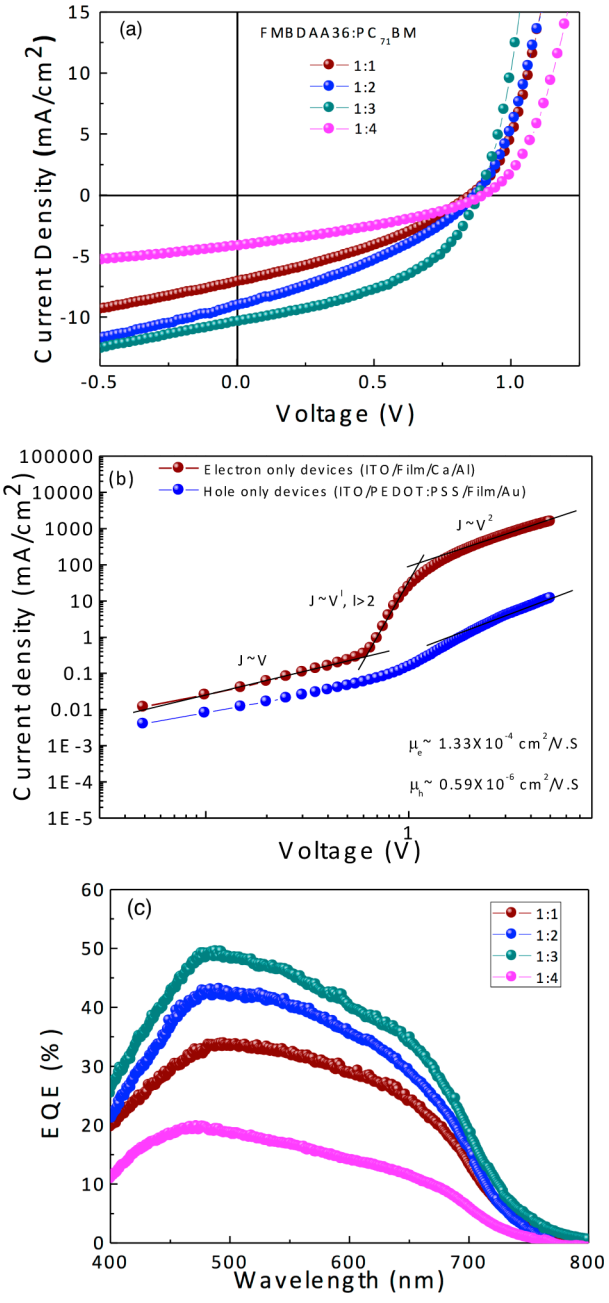


**Figure 3.** (a) Current density−voltage characteristics of the devices for different weight ratio of FMBDAA36 and $PC_{71}BM$ under 100 mW/cm$^2$ AM 1.5 simulated solar irradiation. (b) Dark current density vs voltage characteristic of FMBDAA36:$PC_{71}BM$ (1:3) single carrier devices used for hole (Blue curve, ITO/PEDOT:PSS/FMBDAA36:$PC_{71}BM$/Au) and electron (Merlot curve, ITO/FMBDAA36:$PC_{71}BM$/Ca/Al) mobility measurement. Ohmic $J \propto V$, space charge $J \propto V^2$, and trap-filled $J \propto V^l$, $l > 2$ is indicated by lines fitted in those regions to eq 1 in the text. (c) External quantum efficiency (EQE) spectra of the corresponding devices.

showed matching of energy levels to within 0.1 eV for PEDOT:PSS and FMBDAA36 within the resolution limit of the instrument, with E(HOMO) = 5.2−5.3 eV and 5.2−5.25 eV, respectively. OPV device fabrication with a single solvent made optimization of spin coating speed, and of the FMBDAA36:$PC_{71}BM$ ratio and overall solution concentration both straightforward and reproducible. The optimum performance was found for a 1:3 w:w FMBDAA36:$PC_{71}BM$ ratio (Table 1, Figure 3), giving a PCE of $\eta$ = 4.1% with open circuit voltage $V_{OC}$ = 0.89 V, short circuit current $J_{SC}$ = 10.35 mA cm$^{-2}$, and fill factor FF = 44.8%. In other work to make solvent-fabricated devices with molecular OPV substrates, use of good/bad solvent mixtures (relative to solubility of the active layer components) has proven useful to optimize PCE by creating an appropriate bulk heterojunction (BHJ) active layer morphology of intermingled electron donor and acceptor phases for best photocharge generation and transport.[2,3,7,] Use of small amounts of solvent additives has also become part of this approach.[8,9] But, use of this good/bad mixed solvent approach to give a BHJ phase separation of FMBDAA36 from $PC_{71}BM$ was not effective, since both components were reasonably soluble in commonly used organic solvents, including dichlorobenzene, chlorobenzene, chloroform, and toluene. Using these solvents, device performance remained almost the same using single-solvent or mixed-solvent fabrication procedures.

Dark current measurements indicated the modest fill factor in the optimized device to be due to unbalanced charge flow, with much higher electron than hole mobility, $\mu_{e-} = 133 \times 10^{-6}$ cm$^2$/(V·S) versus $\mu_{h+} = 0.59 \times 10^{-6}$ cm$^2$/(V·S) (Figure 3b). Part of this is due to $PC_{71}BM$ being in *molar* excess at a molar ratio of 2.2:1 relative to FMBDAA36. The electron and hole mobilities were estimated using Child's law in eq 1 from space charge limited current (SCLC)[10,11]

$$J_{SCLC} = \frac{9}{8}\varepsilon_r\varepsilon_0\mu\frac{V^2}{L^3} \quad (1)$$

where $\varepsilon_r$ relative dielectric constant, $\varepsilon_0$ is is the permittivity of free space, $L$ is the film thickness in nanometers (~80 nm here), and $V$ is the applied voltage. Hole-only and electron-only devices were fabricated with the following configurations: ITO/PEDOT:PSS/FMBDAA36:$PC_{71}BM$/Au and ITO/FMBDAA36:$PC_{71}BM$/Ca/Al, respectively. Three well-defined *J-V* characteristic regions (ohmic $J \propto V$, space charge $J \propto V^2$, trap-filled $J \propto V^l$, $l > 2$) are indicated in Figure 3b with lines fitted in those regions to eq 1; this behavior was seen for all devices tested. The hole and electron mobilities were calculated from the space charge limited current region. External quantum efficiency (EQE) measurements also show best performance for the 1:3 w:w FMBDAA36:$PC_{71}BM$ ratio (Figure 3c), as well as an enhanced contribution to PCE in the longer wavelength 600−750 nm portion of the spectrum relative to the thin film absorbance profile (Figure 1).

Despite their modest FF, the FMBDAA36:$PC_{71}BM$ devices show promise because of their reasonably good PCE and straightforward, readily reproduced fabrication procedure. In an effort to probe whether a BHJ phase-separated morphology forms in the FMBDAA36:$PC_{71}BM$ active layers, they were examined by conductive atomic force microscopy (c-AFM) mapping,[12] which was done simultaneously with topographic height imaging (AFM samples were prepared in the same manner as for OPV evaluation, but without adding the LiF layer or Al cathode). Measurements were carried out in contact mode with constant deflection in order to maintain contact during a raster scan. A bias of −9.00 V was applied between the Pt coated probe and the sample ITO electrode, to evaluate hole current from the probe to the electrode. Figure 4 shows the local heterogeneity for c-AFM maps of FMBDAA36:$PC_{71}BM$ films prepared in the manner used for OPV device testing. Areas of high hole conduction are shown in blue and low hole

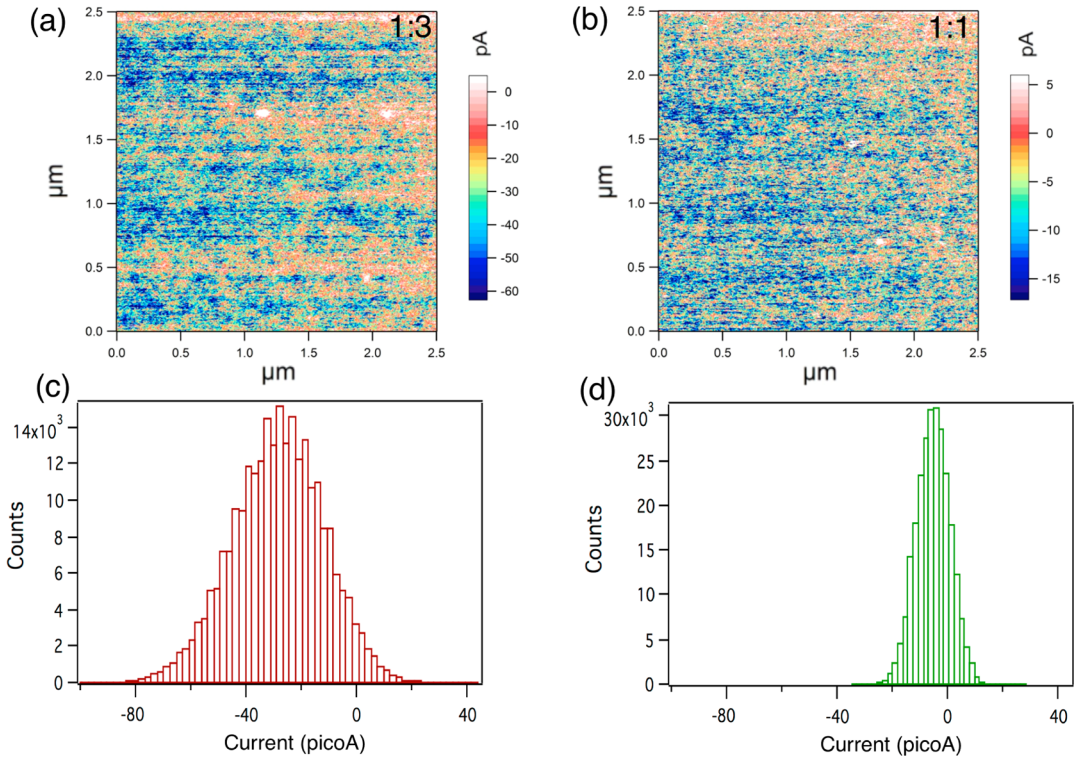


**Figure 4.** c-AFM hole transport maps for (a) 1:3 w:w and (b) 1:1 w:w FMBDAA36:$PC_{71}BM$ films spin-coated from chlorobenzene on an ITO substrate coated with PEDOT:PSS, with (c, d) corresponding current distribution histogram for number of pixels vs current of the c-AFM maps. Measurements used a −9.00 V potential from ITO substrate to Pt coated probe. Mapped area a has an average rms current roughness of 33.5 pA, and b has an average rms current roughness of 8.3 pA.

conduction in orange, with corresponding current distribution histograms.

The 1:3 film showed higher overall hole current than the 1:1 film, indicating better hole mobility in the sample. Assuming that films compared by c-AFM have essentially the same thickness, the higher current regions show that the pathways for hole transport have lower resistance there. We speculate that phase separation from $PC_{71}BM$ forces FMMDAA36 into morphological structures that provide shorter paths for hole conduction. The 1:3 film also showed a greater local hole conduction heterogeneity with a broader current distribution than the 1:1 film, as shown in Figure 4c−d. Wider current distributions in current maps as in Figure 4a have been reported to correlate with better OPV device performance.[13] More generally, c-AFM of the films showed a granular separation of regions with high versus low hole transport, suggesting BHJ type phase separation of FMBDAA36 and $PC_{71}BM$, respectively (or at least regions that are enriched in these components). The observed local current heterogeneity was on the 10−100 nm scale which tends to be most effective[11] for OPV performance. A fibrillar structure has been reported for active layer films of some polymer based OPV devices,[14,15] especially[16] P3HT-based devices. The granular appearance of films in the present study is much different, possibly due to crystallite formation as chlorobenzene evaporates from the spin coated FMBDAA36:$PC_{71}BM$ mixture. The images in Figure 4a, b presumably are influenced by both charge flow and surface topography effects, but the tapping mode AFM shows topographically quite smooth surfaces for both 1:3 and 1:1 FMBDAA36:$PC_{71}BM$ films, with rms roughnesses <0.5 nm (see examples in the Supporting Information, Figure S6). So, it is reasonable that the granularity of Figures 4a-b realistically reflects the BHJ nature of effective charge flow variation in the films. The relatively high potential needed to measure the c-AFM granular hole transport behavior suggests that $PC_{71}BM$ may be enriched at the top of the fabricated active layer,[17,18] giving a smoother surface roughness with good contact of this electron transport phase with the cathode.

In the closest comparison to the present study, Chi et al. reported[19] making the analogue FMBTol36 of FMBDAA36 having methyl instead of methoxy groups. Its absorption characteristics were similar to those of FMBDAA36, and were attributed to intramolecular charge transfer character. Like FMBDAA36, FMBTol36 exhibited crystallographic FM group $\pi$-stacking (at a distance of 3.42 Å); the similarity of crystallographic motifs is notable. The arylamine-substituted fluorenylidene malononitriles may favor $\pi$-stacking without much stack slippage, because bulky arylamino substituents force the FM groups into stacking. The Cambridge Structure Database[20] shows that other fluorenylidene malononitriles tend much more toward slip-stacking rather than the columnar $\pi$-stacking seen in these compounds (see a brief summary at the end of the Supporting Information). No additional 3,6-disubstituted fluorenylidene malononitrile crystallography reports were found, so this class of molecules merits further study.

Instead of the solution-fabrication methods used in the present study, Chi et al. made single-stack devices by thermal layer deposition in an ITO/$MoO_3$/{1:1 FMBTol36:(C60 or C70)}/(C60 or C70)/bathocuproine/Ag configuration. They found essentially the same PCE (4.04%) that we obtained with FMBDAA36 by solution fabrication, with slightly higher $V_{OC}$ and FF, and rather lower $J_{SC}$. The $V_{OC}$ from FMBTol36 is slightly higher than in FMBDAA36, although the two


dx.doi.org/10.1021/am504993j | ACS Appl. Mater. Interfaces 2014, 6, 16476−16480

compounds have essentially the same HOMO energy. The good results achieved by both solution fabrication in the present work, and thermal deposition in the work by Chi et al., together encourage prospects to use both fabrication methods to tune OPV device design readily and effectively with the molecular components, especially for multistack devices requiring good layer orthogonality.

In summary, we report a straightforward, single solvent solution fabrication of a bulk heterojunction solar cell giving power conversion efficiency just over 4% using FMBDAA36 and $PC_{71}BM$. The fluorenylidene malononitriles are remarkably simple molecular species with promising optoelectronic and electrochemical properties. The promisingly good PCE obtained in all-molecular solar cells with the few examples tested in this family of molecules makes them good candidates for further testing to give additional increases in solar conversion efficiency. The formation of a bulk heterojunction morphology in FMBDAA36:$PC_{71}BM$ mixtures from simple spin coating fabrication is remarkable, and should impel efforts to see whether other fluorenylidene malononitrile derivatives may be similarly cooperative, such as systems reported earlier by Homnick et al.[5] that are presently under further investigation.

## ■ ASSOCIATED CONTENT

### Supporting Information

Preparation and crystallographic/$^1$H NMR/UPS characterization of FMBDAA36; experimental details of device fabrication and evaluation; AFM/c-AFM measurement details and example surface images. CCDC Deposition Nr. 1016267 reports supplementary crystallographic data for this article. This material is available free of charge via the Internet at http://pubs.acs.org.

## ■ AUTHOR INFORMATION

### Corresponding Author

* E-mail: lahti@chem.umass.edu.

### Notes

The authors declare no competing financial interest.

## ■ ACKNOWLEDGMENTS

This work was supported as part of Polymer-Based Materials for Harvesting Solar Energy, an Energy Frontier Research Center funded by the U.S. Department of Energy, Office of Science, Basic Energy Sciences under Award DE-SC0001087. J.T.M. gratefully acknowledges the support of NSF-MRI Grant 1228232 for the purchase of a diffractometer.

## ■ REFERENCES

(1) Chen, Y.-H.; Lin, L.-Y.; Lu, C.-W.; Lin, F.; Huang, Z.-Y.; Lin, H.-W.; Wang, P.-H.; Liu, Y.-H.; Wong, K.-T.; Wen, J.; Miller, D. J.; Darling, S. B. Vacuum-Deposited Small-Molecule Organic Solar Cells with High Power Conversion Efficiencies by Judicious Molecular Design and Device Optimization. *J. Am. Chem. Soc.* **2012**, *134*, 13616−13623.

(2) Roncali, J. Molecular Bulk Heterojunctions: An Emerging Approach to Organic Solar Cells. *Acc. Chem. Res.* **2009**, *42*, 1719−1730.

(3) Kyaw, A. K. K.; Wang, D. H.; Luo, C.; Cao, Y.; Nguyen, T.-Q.; Bazan, G. C.; Heeger, A. J. Effects of Solvent Additives on Morphology, Charge Generation, Transport, and Recombination in Solution-Processed Small-Molecule Solar Cells. *Adv. Energy. Mater.* **2014**, *4*, 1301469/1−9.

(4) Kyaw, A. K. K.; Wang, D. H.; Gupta, V.; Leong, W. L.; Ke, L.; Bazan, G. C.; Heeger, A. J. Intensity Dependence of Current−Voltage Characteristics and Recombination in High-Efficiency Solution-Processed Small-Molecule Solar Cells. *ACS Nano* **2013**, *7*, 4569−4577.

(5) Homnick, P. J.; Tinkham, J. S.; Devaughn, R.; Lahti, P. M. Engineering Frontier Energy Levels in Donor-Acceptor Fluoren-9-ylidene Malononitriles versus Fluorenones. *J. Phys. Chem. A* **2014**, *118*, 475−486.

(6) Estrada, L. A.; Neckers, D. C. Synthesis and Photophysics of Ambipolar Fluoren-9-ylidene Malononitrile Derivatives. *J. Org. Chem.* **2009**, *74*, 8484−8487.

(7) Ferdous, S.; Liu, F.; Wang, D.; Russell, T. P. Solvent Polarity Induced Active Layer Morphology Control in Crystalline Diketopyrrolopyrrole-based Low Band Gap Polymer Photovoltaics. *Adv. Energy Mater.* **2014**, *4*, 1300834/1−10.

(8) Liao, H. C.; Ho, C. C.; Chang, C. Y.; Jao, M. H.; Darling, S. B.; Su, W. F. Additives for Morphology Control in High-Efficiency Organic Solar Cells. *Mater. Today.* **2013**, *16*, 326−336.

(9) Kyaw, A. K. K.; Wang, D. H.; Luo, C.; Cao, Y.; Nguyen, T.-Q.; Bazan, G. C.; Heeger, A. J. Effects of Solvent Additives on Morphology, Charge Generation, Transport, and Recombination in Solution-Processed Small-Molecule Solar Cells. *Adv. Energy Mater.* **2014**, *4*, 1301469/1−9.

(10) Lampert, M. A.; Mark, P. *Current Injection in Solids*; Academic Press: New York, 1970.

(11) Chirvase, D.; Chiguvare, Z.; Knipper, M.; Parisi, J.; Dyakonov, V.; Hummelen, J. C. Temperature Dependent Characteristics of Poly(3 hexylthiophene)-fullerene Based Heterojunction Organic Solar Cells. *J. Appl. Phys.* **2003**, *93*, 3376−3383.

(12) Pingree, L. S. C.; Reid, O. G.; Ginger, D. S.; Ginger, D. S. Imaging the Evolution of Nanoscale Photocurrent Collection and Transport Networks during Annealing of Polythiophene/Fullerene Solar Cells. *Nano Lett.* **2009**, *9*, 2946−2952.

(13) Groves, C.; Reid, O. G.; Ginger, D. S. Heterogeneity in Polymer Solar Cells: Local Morphology and Performance in Organic Photovoltaics Studied with Scanning Probe Microscopy. *Acc. Chem. Res.* **2010**, *43*, 612−620.

(14) Liu, F.; Zhao, W.; Tumbleston, J. R.; Wang, C.; Gu, Y.; Wang, D.; Briseno, A. J.; Ade, H.; Russell, T. P. Understanding the Morphology of PTB7:PCBM Blends in Organic Photovoltaics. *Adv. Energy Mater.* **2014**, *4*, 1301377/1−9.

(15) Wang, H.-W.; Pentzer, E.; Emrick, T.; Russell, T. P. Preparation of Low Band Gap Fibrillar Structures by Solvent-Induced Crystallization. *ACS Macro Lett.* **2014**, *3*, 30−34.

(16) Yang, X.; Loos, J.; Veenstra, S. C.; Verhees, W. J. G.; Wienk, M. M.; Kroon, J. M.; Michels, M. A. J.; Janssen, R. A. J. Nanoscale Morphology of High-Performance Polymer Solar Cells. *Nano Lett.* **2005**, *5*, 579−583.

(17) van Bavel, S. S.; Sourty, E.; de With, G.; Loos, J. Three-Dimensional Nanoscale Organization of Bulk Heterojunction Polymer Solar Cells. *Nano Lett.* **2009**, *9*, 507−513.

(18) Chen, D.; Liu, F.; Wang, C.; Nakahara, A.; Russell, T. P. Bulk Heterojunction Photovoltaic Active Layers via Bilayer Interdiffusion. *Nano Lett.* **2011**, *11*, 2071−2078.

(19) Chi, L.-C.; Chen, H.-F.; Hung, W.-Y.; Hsu, Y.-H.; Feng, P.-C.; Chou, S.-H.; Liu, Y.-H.; Wong, K.-T. Donor-Acceptor Small Molecule with Coplanar and Rigid P-bridge for Efficient Organic Solar Cells. *Sol. Energy Mater. Sol. Cells* **2013**, *109*, 33−39.

(20) Allen, F. H. The Cambridge Structural Database: a Quarter of a Million Crystal Structures and Rising. *Acta Crystallogr., Sect. B* **2002**, *58*, 380−388.